IEEE Access
Multidisciplinary | Rapid Review | Open Access Journal

Received May 26, 2020, accepted May 31, 2020, date of publication June 5, 2020, date of current version June 25, 2020.

Digital Object Identifier 10.1109/ACCESS.2020.3000436

A Compact Multiband Printed Monopole Antenna With Hybrid Polarization Radiation for GPS, LTE, and Satellite Applications

MOHAMMED A. AL-MIHRAB[1], ALI J. SALIM[2], AND JAWAD K. ALI[2], (Senior Member, IEEE)
[1]Department of Electronic and Communication Engineering, Cankaya University, 06790 Ankara, Turkey
[2]Microwave Research Group, Department of Electrical Engineering, University of Technology, Baghdad 10066, Iraq

Corresponding author: Mohammed A. Al-Mihrab (c1582654@student.cankaya.edu.tr)

ABSTRACT A new compact printed monopole antenna is presented in this paper. An open-loop hexagonal radiator excited by a microstrip feed line, which is printed on top of the substrate, which is FR4 type, while on another side, a partial ground plane is fixed and embedded with two pairs of slits as well as a pair of rectangular strips. Triple operating bands with two different polarization types are obtained. The lower band has right-hand circular polarization (RHCP) characteristic, whereas the upper band has left-hand circular polarization (LHCP) characteristic means that a dual-band dual-sense circular polarization (CP). Concerning the middle band, a linear polarization (LP) has been gotten in this antenna. Numerical analysis and experimental validation of the proposed antenna structure have been performed, and results are demonstrated. The measured impedance bandwidths (IBWs) are 14.7% (1.478-1.714 GHz), 6.8% (2.54-2.72 GHz), and 13.1% (4.29-4.89 GHz), respectively. The measured 3-dB axial ratio bandwidths (ARBWs) are 6.2% (1.510-1.606 GHz), and 22.7% (4.035-5.07 GHz) for the lower and the upper band, respectively. So, it's suitable for covering modern wireless applications such as GPS (Global Positioning System), LTE (Long Term Evaluation), and Satellite.

INDEX TERMS Hybrid polarization, dual-band dual-sense CP, printed monopole antenna, axial ratio, linear polarization.

I. INTRODUCTION

During the last decade, wireless communication systems have been grown significantly. This development comes spontaneously due to the increased functionality of wireless devices. It is well known that the antennas represent the backbone of wireless communication systems. The polarization variety in printed antennas gives a significant possibility in the multiplicity of applications used in wireless communication systems. Some of these systems constructed depending on linear polarization (LP) [1], [2], whereas others build based on circular polarization (CP) [3]–[5]. On the other hand, other applications have used both polarizations (CP and LP) such as wireless local area networks (WLAN) and worldwide interoperability for microwave access (WiMAX) to benefit from provided frequency. This matter led to design printed antennas with multiband and hybrid polarization. The circular polarization (CP) antennas have distinct features as compared to linear polarization (LP). The first feature, it is very influential in struggling multi-path interferences or fading so, it's granular for the harsh environment such as high humidity and rainy. Second, CP antennas can improve the root mean square time delay spread [6], [7].

Various kinds of dual-band monopole antennas with different shapes are presented in [8]–[19]. In [8], [9], a single-sense CP is demonstrated while in [10]–[15], dual-sense CP monopole antennas excited by microstrip feedline are presented. Regarding [8], the antenna is implemented by loading two L-shaped stubs outside the truncated patch, which excited by meandering probe feed, whereas in [9], a rectangular strip embedded with two slits excited by direct feedline printed on a substrate. On the other side, a reduced ground plane with pair sleeves is extended from its edges.

In [10], a dual-band dual-sense CP achieved via etching annular slot with four unequal arms etched on one side of a substrate while a microstrip feed line printed on another side. In [11], an annular slot, pair of notches, and asymmetrical cross slots are printed on a single substrate, whereas on the other side, the rectangular strip is excited by a direct feedline to perform dual-band dual-sense CP. In [12],

The associate editor coordinating the review of this manuscript and approving it for publication was Yingsong Li.

Two concentric annular slots with reactively loaded etched from patch while on another side, the microstrip feed line which based on stepped impedance employed to produce dual-band dual-sense CP. In [13], a dual-band dual-sense CP generated by etching asymmetrical T slot in the center of the radiator patch as well as truncated triangle strips from opposite corners and a pair of the vertical slot. In [14], a C-shaped radiator printed on the substrate and excited by direct feedline while wide slot with two asymmetrical strips in the opposite direction on the other side used for achieving dual band dual-sense CP. In [15], a tilted D-shaped radiator fed by a microstrip feed line with a suitable impedance transformer and a reduced ground plane on the other side has been configured to perform dual-band dual-sense CP.

Another design approach to fulfill a dual-band dual-sense CP is a slotted ground plane with some perturbations and coplanar waveguide (CPW) feed [16]–[19]. In [16], a slot antenna fed by CPW with pair spiral slots embedded in top left and bottom left corner in the ground plane. In [17], a CPW-fed slot antenna with a U-shaped open-slot and a vertical grounded stub is configured. In [18], a slot square antenna is proposed with a pair of asymmetrical strips added on the ground plane with an F-shaped feed line and parasitic elements configuration. In [19], a dual-band dual- sense created by a rectangular radiator with two unlike rectangular strips excited by CPW surrounded with a square slot ground plane with inverted L-shaped on the right side of it.

Also, there are other approaches used to produce more than one band CP, such as stacking [20]–[25] and metamaterials [26]–[28]. In [20], a pair of stacked patches with low-temperature cofired ceramic (LTCC) substrate type has been constructed to implement a dual-band for GPS application. In [21], an antenna has been configured with two truncated stacked patches, which are excited by coaxial probe-fed to achieve dual-band CP for ISM applications. A microstrip antenna constructed by pair of truncated and semi-groove stacked patches to execute a dual-band CP has been proposed in [22]. Also, in [23], a microstrip antenna configured by a pair of substrate layers separated by an air gap, the rectangular patch printed on top of an upper substrate while the circular patch placed on the other side of it to achieve dual-band CP. Besides, the authors in [24] have presented a double layer microstrip antenna with a rectangular ring below the meandered ring to generate a dual-band resonant response. Moreover, dual pairs of inverted-L shaped strips and perturbation structures are inserted in two rings to perform CP radiation at the two bands. The authors of [25] have investigated the design of a microstrip antenna to obtain dual-band dual-sense CP for UHF RFID reader applications. The proposed antenna is constituted of a pair of elliptical rings, three substrate layers, and an asymmetric Π-type dual-band complex impedance transformer.

In this paper, a multiband printed monopole antenna with dual-band dual-sense CP is investigated. These bands come from a configured monopole antenna with an open-loop hexagonal ring radiator on the top side of a substrate, whereas on the other side, a reduced ground plane with two pairs of slits and one pair of rectangular strips with dimensions of nh1×nw1 and nh2×nw2 have been embedded.

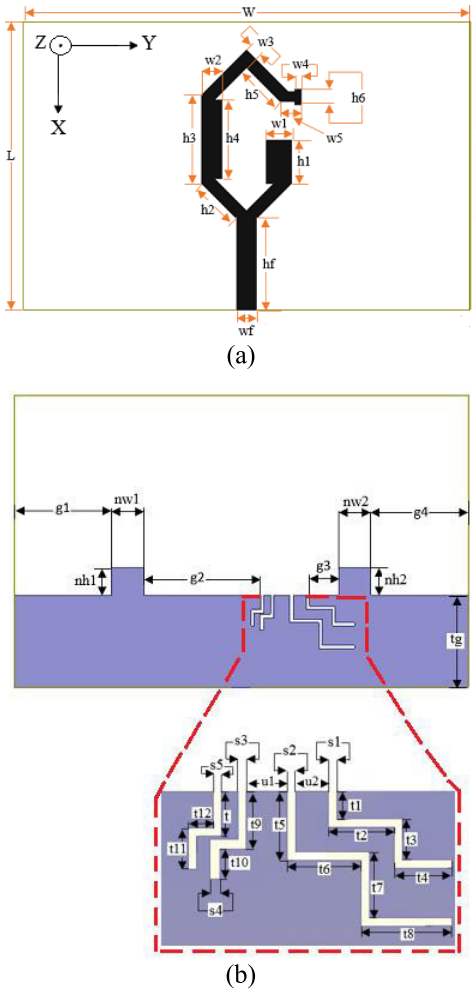

FIGURE 1. Configuration of the proposed open-loop monopole printed antenna (a) radiator part, (b) partial ground plane with stair slits.

II. ANTENNA DESIGN AND ANALYSIS

A. ANTENNA CONFIGURATION

The schematic order of the proposed monopole printed antenna is presented in Fig. 1. The antenna is constituted of three main parts: a ground plane, a dielectric substrate, and a radiator. Regarding the ground plane, it's a partial plane with a pair of rectangular strips with dimensions of nh1×nw1 and nh2×nw2, as well as two pairs of asymmetrical stair slits. The second part is the dielectric substrate with FR4 type ($\varepsilon_r = 4.4$) with thickness 1.6 mm and loss tangent tan δ = 0.02. The last part is the open-loop hexagonal radiator, which excited by a microstrip feed line 50 Ω with a width of wf and length hf. The overall dimensions of the antenna are $70 \times 45 \times 1.6\ mm^3$. The optimized parameters of the proposed printed monopole antenna, using the HFSS V.13 (High Frequency Structure Simulator), are mentioned in Table 1 and Table2.

TABLE 1. Parameters of the proposed antenna.

Parameter	Value (mm)	Parameter	Value (mm)
L	45	h5	7.41
W	70	h6	2.5
w1	4.07	hf	14.42
w2	3.27	g1	15
w3	2	g2	18
w4	1	g3	4.5
w5	2.25	g4	15
wf	3	tg	14.2
h1	6.75	nh1	4.3
h2	7.52	nh2	4.3
h3	13.75	nw1	5
h4	12.24	nw2	5

TABLE 2. Parameters of stair slits.

Parameter	Value (mm)	Parameter	Value (mm)
t1	1.7	t11	2.5
t2	4	t12	1.5
t3	2.5	t	2.7
t4	3.5	s1	0.5
t5	4.2	s2	0.5
t6	4.5	s3	0.5
t7	4	s4	0.6
t8	5.5	s5	0.5
t9	3.5	u1	2.5
t10	1.8	u2	2

B. DESIGN PROCEDURE

This section clarifies the construction stages of the proposed antenna. As illustrated in Fig. 2, the antenna passed in five main stages. At first, the Ant.1, as shown in Fig. 2, its radiator is a hexagonal closed-loop, and the ground part is a partial patch. The primal results of Ant.1 are presented in Fig. 3: there are two operating bands and resonating at around 2.2 GHz and 6 GHz frequencies while the AR level at these bands is very high. In Ant.2, the closed hexagonal radiator ring is opened, which causes to moving reflection coefficient response to the lower frequency region as well as generating another operating at (2.85-3.15 GHz). Regard the AR in Ant.2; the AR level starts to decrease, as noted in Fig. 3(b) and CP condition verified at (4.45-4.67 GHz). For decreasing the AR level at other bands, some of the load parts

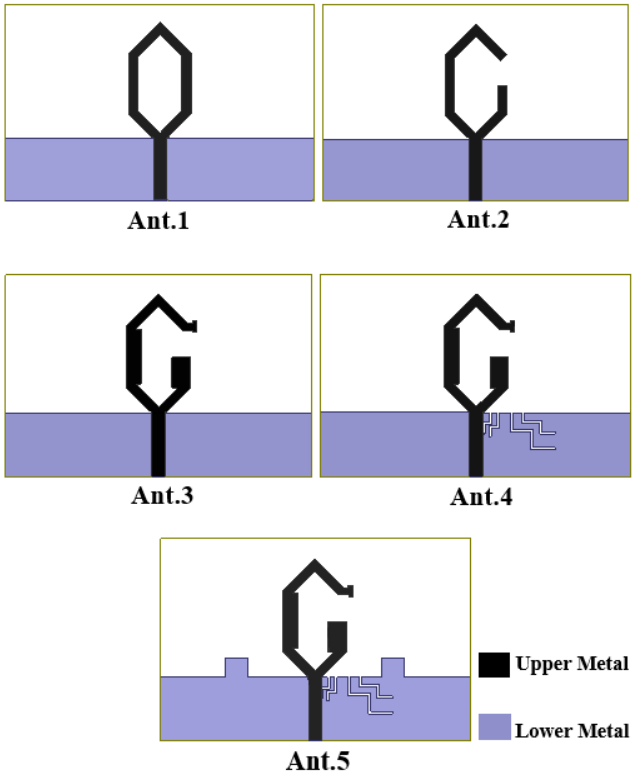

FIGURE 2. Evolution of the proposed open-loop monopole printed antenna.

are added to the radiator part, as shown in Ant.3. Because of loading parts addition, the AR level is decreased under 3dB in another region (6.5-6.8 GHz), as seen in Fig. 3(b), while the reflection coefficient under −10 dB has remained poor. In Ant.4, four stair slits are etched on the ground plane. The necessity of more than one slit in the proposed antenna came because the antenna operates in more than one frequency region. Also, it has an attractive feature to produce different polarizations. Besides, the slits with stair shape are effective in contributing to reduce the axial ratio in band1 and enhancement of it in band4, as shown in Fig. 3. Subsequently, the slits can play a critical role in controlling the polarization of the antenna. In Ant.5 (proposed antenna), a pair of rectangular strips with dimensions of nh1×nw1 and nh2×nw2 have emerged from the partial ground plane. As a result, axial ratio bandwidth (ARBW) is increased from 4.8% to 23.2% at the upper band. Furthermore, the |S11| response became more matchable with AR response at CP bands, as seen in Figs. 3(a) and 3(b). The effect of each part will clarify adequately in the parametric study section.

C. SURFACE CURRENT DISTRIBUTIONS

Surface current distributions are necessary for expounding circular polarization radiation behavior. The current distributions performed on Ant.5 (proposed) at both CP resonant frequencies 1.575 GHz and 4.5 GHz, as noted in Figs. 4(a) and 4(b) respectively. Figs. 4(a) and 4(b) show the surface current distributions on time instants at $t = 0°$ and $t = 90°$ at 1.575 GHz and 4.5 GHz, respectively.

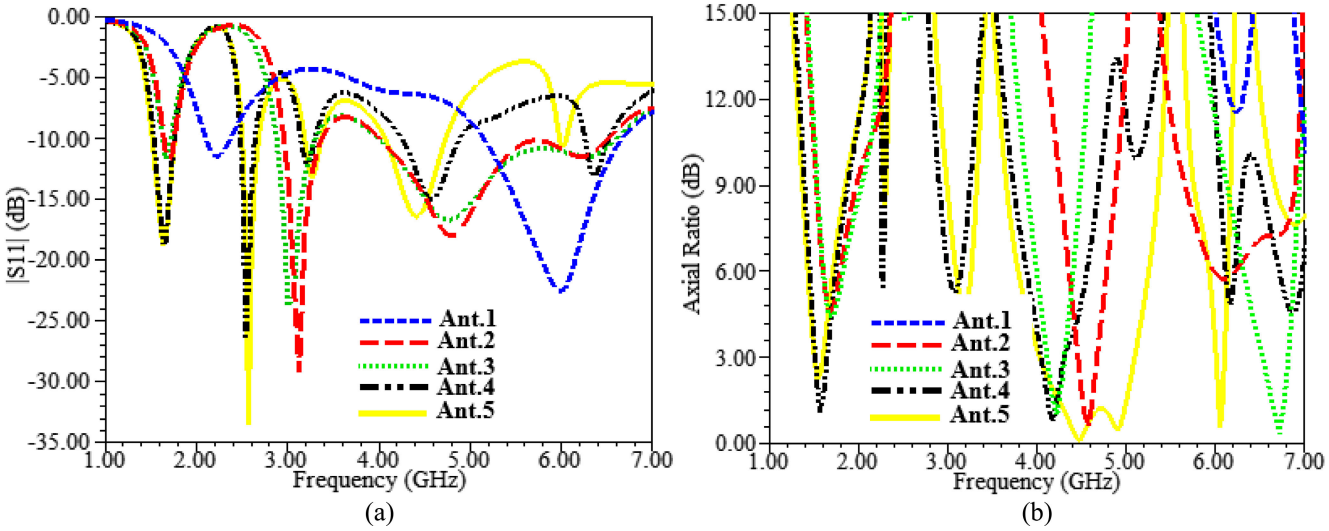

FIGURE 3. Comparison for different stages of Fig. 2 (a) reflection coefficient (|S11|), (b) axial ratio (AR).

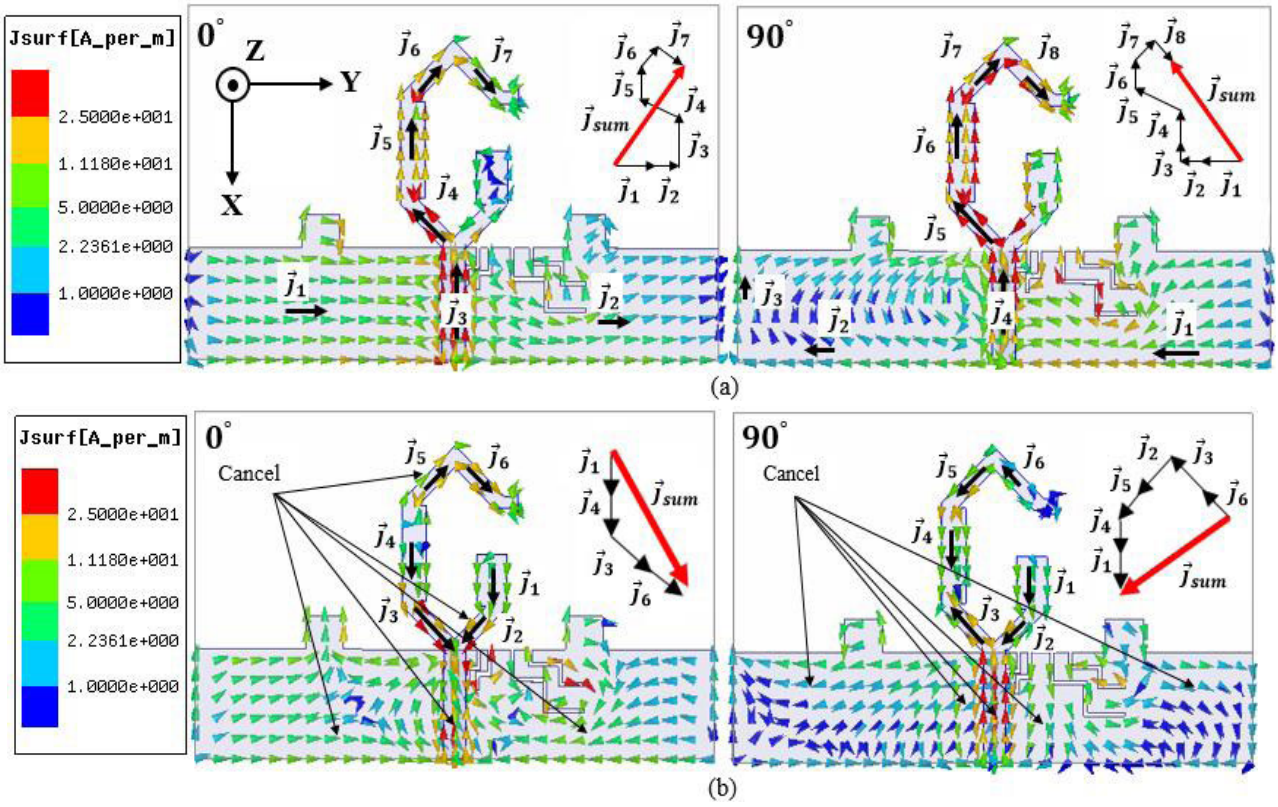

FIGURE 4. The surface current distribution of the proposed open-loop hexagonal radiator antenna at (a) 1.575 GHz, (b) 4.5 GHz.

For verifying CP radiation conditions, the amplitude of vectors should be the same. Besides, the phase difference between these vectors should be 90°. In the proposed antenna, there are two bands that should be CP because the axial ratio is less than 3-dB. By using the current distribution on the proposed antenna, the CP should be verified, and the type of CP should be known for each CP band.

As presented in Fig. 4, the current distributions are implemented at 1.575 GHz and 4.5 GHz when time instants t = 0° and t = 90°. Fig. 4(a) describes the current distributions at 1.575 GHz for t = 0° and t = 90°. As noted in Fig. 4(a), the current intensity focuses on the open-loop hexagonal radiator and ground plane.

Also, CP radiation conditions are observed in many regions. For instance, when t = 0° at 1.575 GHz, CP radiation conditions can be seen between $\vec{j}_6$ and $\vec{j}_7$ in the radiator and around the slit regions in the ground plane. Regarding the 4.5 GHz, when t = 0°, the mentioned conditions can

be perceived for the current vectors $\vec{j}_1$ and $\vec{j}_2$ with $\vec{j}_3$ as shown in Fig. 4(b). Also, the current vectors on stair slits and rectangular strips can contribute significantly to band4 as a CP band.

To investigate of CP in both bands, the current density vector diagram should be obtained. Based on the superposition theorem, the result of the summation vector currents is symbolized with ($\vec{j}_{sum}$). The current vectors and $\vec{j}_{sum}$ represent a conceptual one, not an exact. As much as possible, the length of arrows acts as the current intensity. From Fig. 4 (a), it noted that the type of radiated wave is right-handed circular polarization (RHCP) in the +z-direction because the $\vec{j}_{sum}$ rotates counterclockwise as time increases whereas, in Fig. 4 (b), it noted that the $\vec{j}_{sum}$ rotates clockwise direction as time increases mean that left-handed circular polarization (LHCP) radiation is created in the +z-direction. Another substantial understand from $\vec{j}_{sum}$ is that the lengths of it at t = 0° and t = 90° in both Figs. 4(a) and 4(b) are approaching equality and orthogonality, which explains the CP phenomenon logically. The opposite direction of current vectors with the same magnitude will be canceled, as illustrated in Fig. 4(b).

D. PARAMETRIC STUDY

1) EFFECT OF PARAMETER, W4

The impact of width (w4) on reflection coefficient and axial ratio performance is presented in Figs. 5(a) and 5(b) respectively. Fig. 5(a) clarifies that the parameter w4 impacts only the impedance matching at the middle band at 2.55 GHz. Its effects appear on the axial ratio at the upper band, as shown in Fig. 5(b). The limited increase of w4 from 0 to 1 mm gives a positive result regarding ARBW. The ARBW under 3-dB also raised from 520 MHz to 1.03 GHz means w4 at 1 mm raised the intension of orthogonality of electric field to the maximum.

2) EFFECT OF PARAMETERS, s1 AND s2

The impact of stair slits s1 and s2 on |S11| and AR is illustrated in Figs. 6(a) and 6(b). In the case of s1 = s2 = 0 or s1 = 0.5, s2 = 0, the matched impedance under −10 dB is very poor at the lower band with the absence of a middle band at 2.55 GHz completely. This matter implies that s2 plays a significant role in impedance matching, as well as it's entirely responsible for middle band creation. Regarding s1, its weight displayed at the upper band by shifting and matching. Also, the parameters s1 and s2 have a significant role in producing a circular polarization at the lower band and the upper band. For the lower band, the s1 or s2 is enough to fulfill the CP target, but for the upper band, the maximum ARBW is achieved when s1 and s2 exist together. From the above, the s1 and s2 make an appropriate disturbance in the electric field, which leads to reinforcing the orthogonality.

3) EFFECT OF PARAMETERS, s3, s4, AND s5

The parameters s3, s4, and s5 have a substantial influence on the reflection coefficient and axial ratio, as seen in Figs. 7(a) and 7(b), respectively. As noted in Fig 7, there is a balance between |S11| and AR responses. This came from the investigation of the effect of each parameter independently. The importance of these parameters displayed on the upper band, whether in |S11| or AR. The best-case noted when s4 = 0.5, s3 = 0.5, and s5 = 0.6 because they provide a maximum ARBW as well as produce an acceptable matching impedance in the upper band, which covers entirely with AR lower than 3-dB.

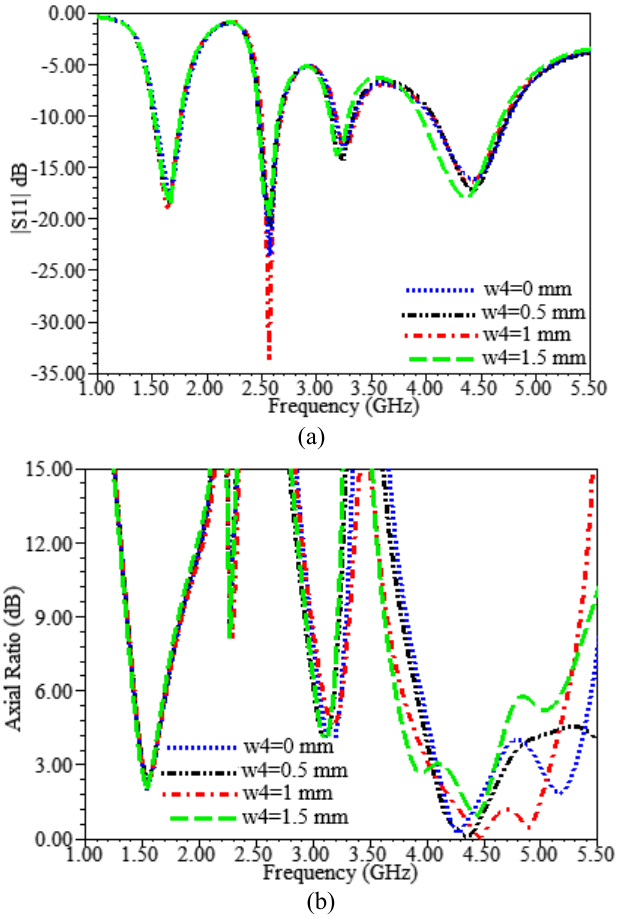

FIGURE 5. Effect of w4 on antenna performance: (a) |S11|, (b) AR.

III. RESULTS AND DISCUSSIONS

A. REFLECTION COEFFICIENT AND AR

In this subsection, the simulated and measured results of the reflection coefficient and the axial ratio are presented. Regarding measurement, first, the proposed antenna is fabricated using CNC3018-3 axis, as shown in Figs. 8(a) and 8(b) then measured by using VNA (vector network analyzer) model (Anritsu, 3650 A), as noted in Fig. 8(c).

AR is the ratio between major to minor axes of the elliptical polarization. The test implemented a linearly polarized antenna rotating about its polarization axis, and the AUT remains fixed until getting maximum measured signal by the spectrum analyzer (MCS Real-Time Spectrum Analyzer Software-Version 1.4.5), afterward, rotating the linearly

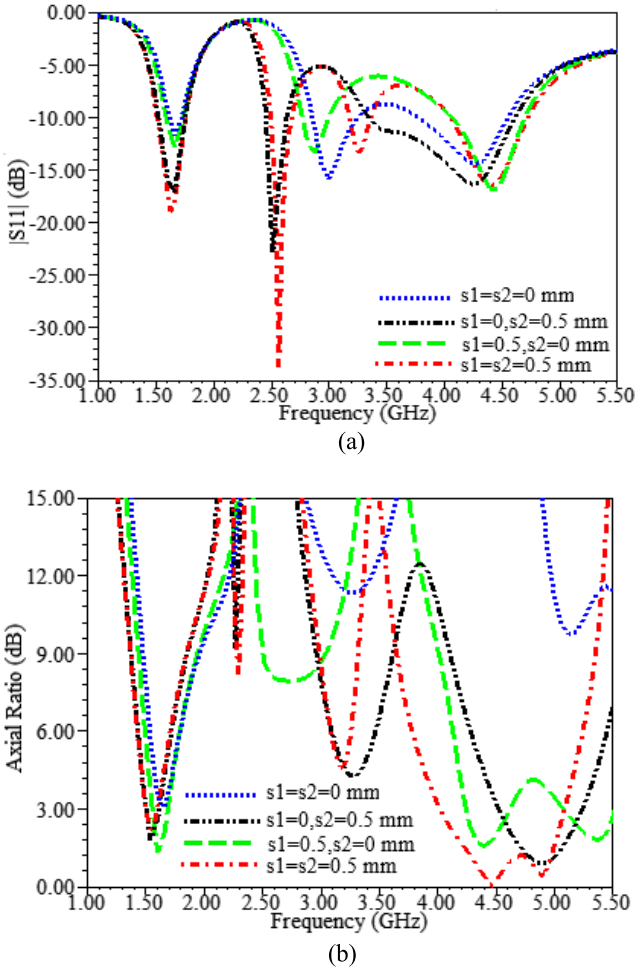

FIGURE 6. Effect of stair slits s1 and s2 on antenna performance: (a) |S11|, (b) AR.

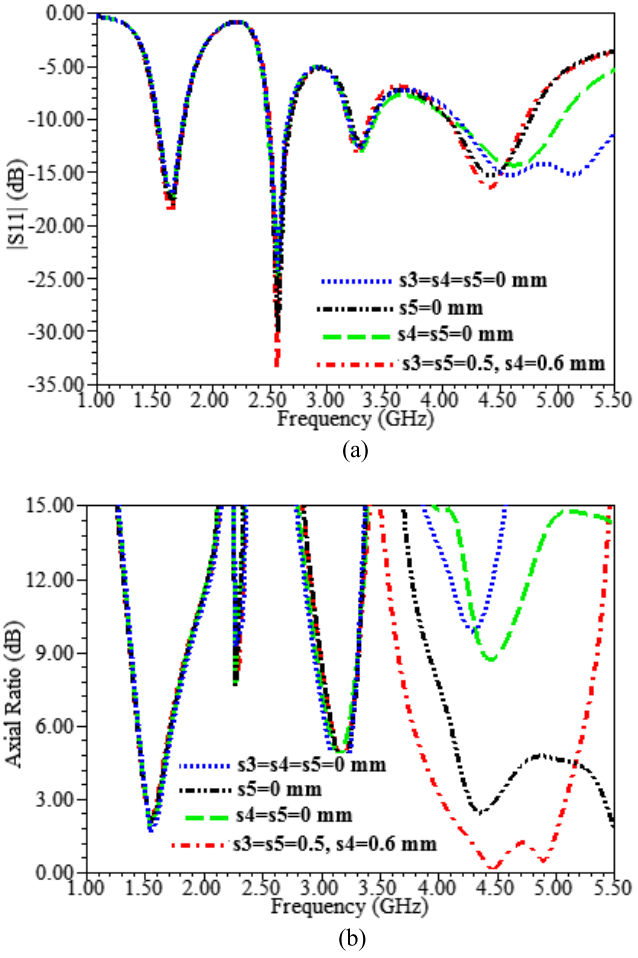

FIGURE 7. Effect of stair slits s3, s4, and s5 on antenna performance: (a) |S11|, (b) AR.

polarized antenna 90° about the same axis to measure the minor axis of the ellipse.

Fig. 9 reveals some critical points. First, it noted that there is a harmony between simulated and measured results at band1 as regard |S11| and AR. At the same time, other bands are slightly shifted towards the high-frequency region due to dielectric material properties of commercially available and SMA connector connectivity. Furthermore, the axial ratio is less than 3-dB at band1 and band4 regions. This means that the antenna can radiate or receive the waves which have the circularly polarized characteristic.

Regarding other middle bands, they are with linear polarization. Band3 can be canceled because it has very poor impedance bandwidth under the −10 dB. The simulated and measured impedance bandwidths (IBWs) for all bands and ARBWs under 3-dB are listed in Table3.

B. GAIN

The gain of the proposed antenna is illustrated in Fig. 10, which demonstrates both simulated and measured results of peak gain, which vary with frequency. The prototype antenna gain is measured employing the 3-antenna technique. Two of them are identical horn antennas (LB-OSJ-20180-P03) are employed for calibration purposes. The powers transmitted and received are seen using MCS Real-Time Spectrum Analyzer Software-Version 1.4.5, as shown in Fig.3. The procedure is repeated after replacing one of the horn antennas with the proposed antenna. The simulated peak gains at band1, band2, and band4 are (1.72-2.63) dBi, (3.85-4.04) dBi, and (4.57-5.52) dBi, respectively whereas, the measured gains for same bands are (1.55-2.53) dBi, (3.35-3.81) dBi, and (4.5-5.45) dBi.

C. THE RADIATION PATTERNS

The simulated and measured results are plotted in both XZ-plane (phi = 0°) and YZ-plane (phi = 90°) at frequencies 1.575 GHz, 2.55 GHz, and 4.5 GHz. The measurement radiation patterns are implemented in a noise-free environment (anechoic chamber) employing two antennas set up. The antenna under test (AUT) is put in a rotating platform, whereas the reference antenna, which is a dual-polarization

TABLE 3. The simulated and measured results of the proposed antenna.

Bands	(Simulated) IBWs (GHz, f2-f1, %)	(Measured) IBWs (GHz, f2-f1, %)	(Simulated) 3-dB ARBWs (GHz, %)	(Measured) 3-dB ARBWs (GHz, %)
Band1	(1.515-1.761), 246, 15	(1.478-1.714), 236, 14.7	(1.508-1.604), 6.2	(1.510-1.606), 6.2
Band2	(2.496-2.679), 183, 7.1	(2.54-2.72), 180, 6.8	None	None
Band3	(3.178-3.363), 185, 5.7	(3.32-3.42), 100, 3	None	None
Band4	(4.054-4.732), 669, 15.2	(4.29-4.89), 600, 13.1	(4.025-5.081), 23.2	(4.035-5.07), 22.7

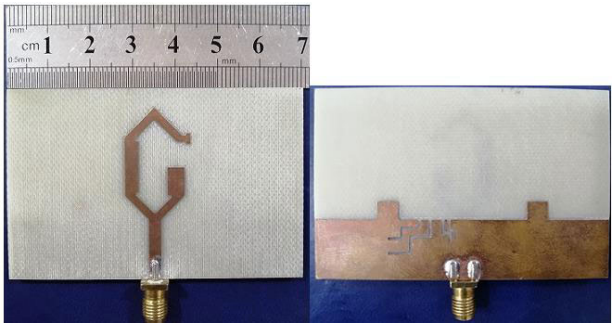

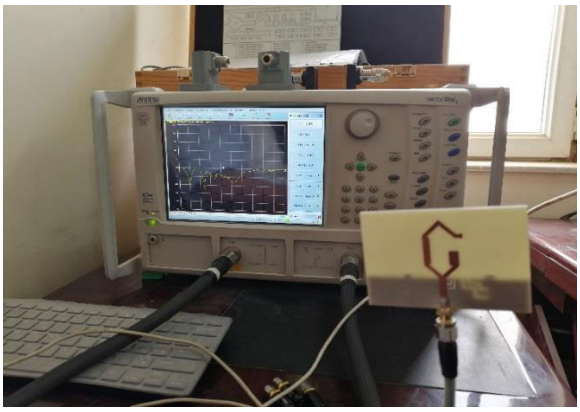

FIGURE 8. The fabricated antenna prototype: (a) top view, (b) bottom view (c) under the VNA test.

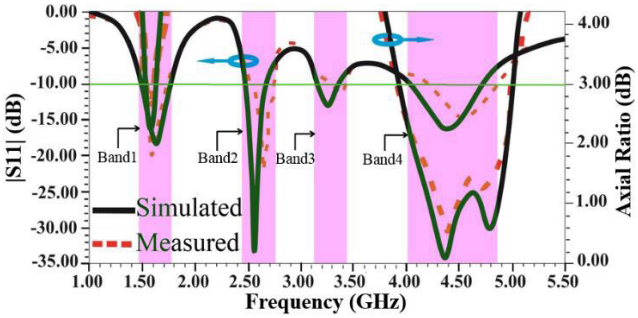

FIGURE 9. Reflection coefficient (|S11|) and AR versus frequency.

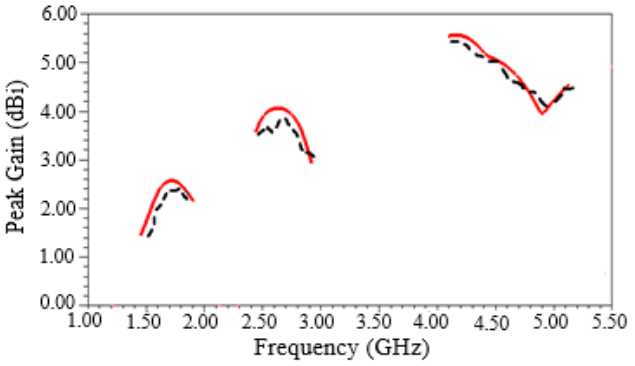

FIGURE 10. Simulated and measured peak gain of the proposed antenna.

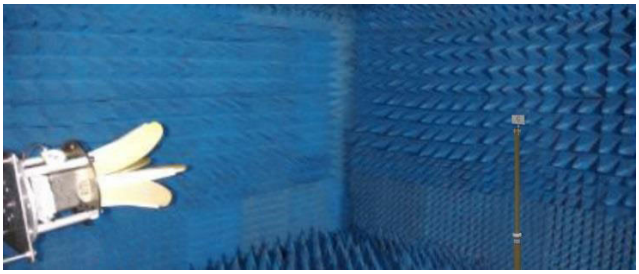

FIGURE 11. The fabricated antenna prototype in the anechoic chamber.

FIGURE 12. The sweep frequency generator type Hewlett Packard 83752B.

type (LB-OSJ-20180-P03), is settled in far-field of (AUT) as shown in Fig. 11. Using the sweep generator (Hewlett Packard 83752B synthesized sweeper) as shown in Fig.12, the test implemented at 1.575, 2.55, and 4.5 GHz and radiation patterns are measured by altering θ from 0° to 360°.

It's observed from Fig. 13(a) that the antenna radiates RHCP wave in +z-direction at 1.575 GHz while LHCP

TABLE 4. Comparison 3-dB beamwidths of the proposed work with previously published works.

Ref.	Polarization type	Antenna type	Band type	3-dB Beamwidth, Freq.(GHz) in XZ-plane	3-dB Beamwidth, Freq.(GHz) in YZ-plane
3	CP	QHA	Broadband	150°, 1.575	None
4	CP	QHA	Single band	174°, 1.575	None
12	CP	Annular slot (Ant.2)	Dual band	99°,1.568 74°, 3788	86°,1.568 86°, 3788
This work	Hybrid	Monopole	Triple	137°, 1.575 188°, 2.55 85°, 4.5	115°, 1.575 110°, 2.55 73°, 4.5

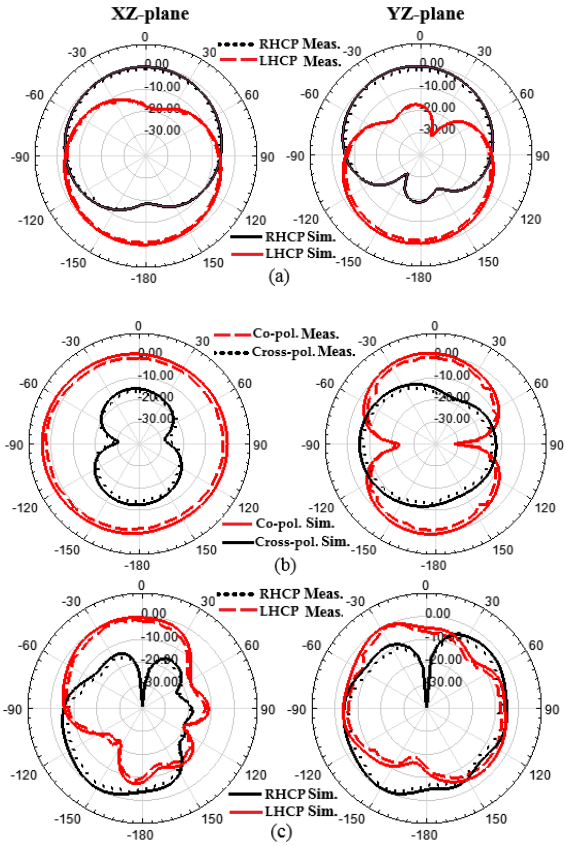

FIGURE 13. Normalized radiation patterns of the proposed antenna at (a) 1.575 GHz, (b) 2.55 GHz, (c) 4.5 GHz.

wave in the −z-direction. When $\theta = 0°$, the simulated and measured cross-polarization level of band1 is about 19dB, which implies a reasonable CP radiation. For 2.55 GHz, the radiation pattern is demonstrated in Fig. 13(b), which describes the radiation shape in both planes. In the XZ-plane, the co-polarization pattern is an omnidirectional shape, whereas it has a bi-directional shape in another plane. Moreover, the difference between co and cross-polarization in the boresight direction is about 15 dB in each plane. As a result, it radiates LP in both planes. The radiation pattern at 4.5 GHz can be noted in Fig.13(c), which indicates that the antenna radiates LHCP wave in the +z-direction and RHCP wave in the opposite direction. Also, it's noted that the pattern shape is slightly tilted from the main axis in both planes because of the asymmetrical geometry of the radiator (open-loop hexagonal). Regarding cross-polarization level in both planes is about 16.5 dB, which shows a satisfactory CP radiation.

Also, the 3-dB beamwidth has been obtained from Fig. 13 for each band in both planes. At band1, the measured 3-dB beamwidths are 137° and 115° in XZ-plane and YZ-plane, respectively. Besides, the radiation pattern deflections at band1 are 3° and 5° in XZ and YZ planes, respectively. Regarding band2 (LTE band), the measured 3-dB beamwidth is larger than band1 and reaches to 188° in XZ-plane while in YZ-plane, the beamwidth is 110°. For the last band (band4), the measured 3-dB beamwidths are 85° and 73° with diverged by 27° and 30° in XZ-plane and YZ-plane, respectively.

Table 4 shows a comparison between the proposed antenna 3-dB beamwidths and previously published works. It shows that the proposed antenna provides large 3-dB beamwidths as compared to the monopole antenna presented in [12] while smaller than quadrifilar helical antenna's beamwidth as expressed in [3], [4].

Table 5 shows the comparison of the proposed antenna performance with other works that have been published recently. The comparison involves some of the essential specifications such as size, ARBWs, feed type, number of layers, and number of bands. The proposed antenna surpasses as compared to others, at least in one specification. Regarding size, the proposed work is compact as compared with others. Furthermore, there is an extra LP band in addition to two CP bands with different senses. Besides, the axial ratio bandwidth under 3-dB of the proposed antenna is more significant than other antennas, which are listed in Table5.

TABLE 5. Comparison of the proposed work with previously published works.

Ref.	Size (mm^2)	Feed type	Number of layers	IBW (GHz, fc, %)	$\|s11\| < -10$ dB Bands	3-dB ARBWs (GHz, fc, %)	3-dB ARBW Bands	Polarization
8	230×210	Meandering probe	Single	1.42-1.6, 1.51, 12 2.14-2.56, 2.35, 18	Dual	1.49-1.53, 1.51, 3 2.34-2.43, 2.38, 4	Dual	RHCP RHCP
10	80×80	Microstrip feed	Single	1.26-1.654, 2.46, 26.7 2.44-2.738, 2.59, 11.3	Dual	1.474-1.566, 1.5, 6.1 2.512-2.677, 2.6, 6	Dual	RHCP LHCP
13	55×55	Microstrip feed	Single	2.494 -2.68, 2.53, 7.2 5.61-5.816, 5.73, 3.6	Dual	2.5-2.557, 2.52, 2 5.61-5.79, 5.65, 3.2	Dual	LHCP RHCP
16	70×70	CPW	Single	1.54-1.68, 1.6, 8.7 1.96-2.47, 2.2, 23	Dual	1.54-1.675, 1.6, 8.4 2.02-2.45, 2, 19	Dual	RHCP LHCP
18	63.5×55	CPW	Single	1.57-2.04, 1.75, 26.04 2.87-3.47, 3.25, 18.93	Dual	1.6-2, 1.8, 22.2 3.15-3.5, 3.325, 10.53	Dual	RHCP LHCP
21	60×60	Probe	Double	2.4-2.5, 2.45, 9.1 4.98-6.5, 5.8, 26.2	Dual	2.42-2.47, 2.45, 1.842 5.72-5.89, 5.8, 2.97	Dual	RHCP RHCP
22	60×60	Probe	Double	2.4-2.53, 2.45, 5.27 5.6-6.15, 5.8, 9.36	Dual	2.428-2.471, 2.45, 1.76 5.877-5.877, 5.8, 2.67	Dual	LHCP LHCP
23	100×100	Aperture	Double	2.015–2.37, 2.19, 16.2 2.64–2.95, 2.79, 11.29	Dual	2.238-2.285, 2.256, 2.1 2.645-2.69, 2.667, 2	Dual	LHCP LHCP
24	80×80	Two coaxial coupled feeding networks	Double	1.595–1.632, 1.61, 2.3 2.395–2.574, 2.45, 7.2	Dual	1.609-1.619, 1.61, 0.6 2.474–2.509, 2.49, 1.4	Dual	LHCP RHCP
This work	70×45	Microstrip feed	Single	1.48-1.714, 1.59, 14.7 2.54-2.72, 2.63, 6.8 4.29-4.89, 4.59, 13.1	Triple	1.51-1.606, 1.558, 6.2 ---------- 4.035-5.07, 4.552, 22.7	Dual	RHCP LP LHCP

IV. CONCLUSION

A compact multiband antenna with dual-band dual-sense circular polarization has been presented. The CP is verified in band1 and band4. The proposed antenna exhibits RHCP at band1 and LHCP at band4. A CP is implemented at these bands due to the effects of parameters s1 and s2. Parameter w4 affects for coupling between axial ratio and reflection coefficient at band4. The pair of rectangular strips in the ground plane has a significant role in increasing the ARBW of band4. Also, the parameters s3, s4, and s5 have affected on reflection coefficient response at band2 as well as AR at band4. Besides, the proposed antenna demonstrated a linear polarization at band2 such that the reflection coefficient has affected by parameter s2. The antenna discriminates with compactness, single layer, direct feed line as well as it provides a new band with LP characteristic that covers an important application. The proposed antenna covers valuable frequency ranges, so; it is an appropriate candidate for various wireless applications such as GPS, LTE, and satellite.

REFERENCES

[1] Y. Li and W. Yu, "A miniaturized triple band monopole antenna for WLAN and WiMAX applications," *Int. J. Antennas Propag.*, vol. 2015, pp. 1–5, Oct. 2015.

[2] J. Li, X. Zhang, Z. Wang, X. Chen, J. Chen, Y. Li, and A. Zhang, "Dual-band eight-antenna array design for MIMO applications in 5G mobile terminals," *IEEE Access*, vol. 7, pp. 71636–71644, 2019.
[3] Y.-S. Wang and S.-J. Chung, "A miniature quadrifilar helix antenna for global positioning satellite reception," *IEEE Trans. Antennas Propag.*, vol. 57, no. 12, pp. 3746–3751, Dec. 2009.
[4] Y. Li and R. Mittra, "A three-dimensional circularly polarized antenna with a low profile and a wide 3-dB beamwidth," *J. Electromagn. Waves Appl.*, vol. 30, no. 1, pp. 89–97, Jan. 2016.
[5] K. L. Chung, Y. Li, and C. Zhang, "Broadband artistic antenna array composed of circularly-polarized wang-shaped patch elements," *AEU-Int. J. Electron. Commun.*, vol. 74, pp. 116–122, Apr. 2017.
[6] S. Gao, Q. Luo, and F. Zhu, "Introduction to circularly polarized antennas," in *Circularly Polarized Antennas*, 1st ed. Chichester, U.K.: Wiley, 2014, ch. 1, pp. 1–2.
[7] Y. Zhang, L. Pang, X. Liang, X. Liu, R. Chen, and J. Li, "Propagation characteristics of circularly and linearly polarized electromagnetic waves in urban macrocell scenario," *IEEE Trans. Veh. Technol.*, vol. 64, no. 1, pp. 209–222, Jan. 2015.
[8] C.-H. Chen and E. K. N. Yung, "A novel unidirectional dual-band circularly-polarized patch antenna," *IEEE Trans. Antennas Propag.*, vol. 59, no. 8, pp. 3052–3057, Aug. 2011.
[9] T.-N. Chang and J.-M. Lin, "Dual-band circularly polarized monopole antenna," *J. Electromagn. Waves Appl.*, vol. 29, no. 7, pp. 843–857, Apr. 2015.
[10] X. Bao and M. J. Ammann, "Dual-frequency dual-sense circularly-polarized slot antenna fed by microstrip line," *IEEE Trans. Antennas Propag.*, vol. 56, no. 3, pp. 645–649, Mar. 2008.
[11] Y. Shao and Z. Chen, "A design of dual-frequency dual-sense circularly-polarized slot antenna," *IEEE Trans. Antennas Propag.*, vol. 60, no. 11, pp. 4992–4997, Nov. 2012.
[12] J. Li, J. Shi, L. Li, T. A. Khan, J. Chen, Y. Li, and A. Zhang, "Dual-band annular slot antenna loaded by reactive components for dual-sense circular polarization with flexible frequency ratio," *IEEE Access*, vol. 6, pp. 64063–64070, 2018.
[13] S. M. Noghabaei, S. K. A. Rahim, P. J. Soh, M. Abedian, and G. A. E. Vandenbosch, "A dual-band circularly-polarized patch antenna with a novel asymmetric slot for WiMAX application," *Radioengineering*, vol. 22, no. 1, pp. 291–295, Apr. 2013.
[14] S. Patil, A. K. Singh, B. K. Kanaujia, and R. L. Yadava, "Design of dual band dual sense circularly polarized wide slot antenna with C-shaped radiator for wireless applications," *Frequenz*, vol. 72, nos. 7–8, pp. 343–351, Jun. 2018.
[15] A. Altaf and M. Seo, "A tilted-D-shaped monopole antenna with wide dual-band dual-sense circular polarization," *IEEE Antennas Wireless Propag. Lett.*, vol. 17, no. 12, pp. 2464–2468, Dec. 2018.
[16] C. Chen and E. K. N. Yung, "Dual-band dual-sense circularly-polarized CPW-fed slot antenna with two spiral slots loaded," *IEEE Trans. Antennas Propag.*, vol. 57, no. 6, pp. 1829–1833, Jun. 2009.
[17] B. Chen and F.-S. Zhang, "Dual-band dual-Sense circularly polarized slot antenna with an open-slot and a vertical stub," *Prog. Electromagn. Res. Lett.*, vol. 48, pp. 51–57, Aug. 2014.
[18] R. K. Saini and P. S. Bakariya, "Dual-band dual-sense circularly polarized asymmetric slot antenna with F-shaped feed line and parasitic elements," *Prog. Electromagn. Res. M*, vol. 69, pp. 185–195, Aug. 2018.
[19] M. Midya, S. Bhattacharjee, and M. Mitra, "CPW-fed dual-band dual-sense circularly polarized antenna for WiMAX application," *Prog. Electromagn. Res. Lett.*, vol. 81, pp. 113–120, Jan. 2019.
[20] S. Chen, G. Liu, X. Chen, T. Lin, X. Liu, and Z. Duan, "Compact dual-band GPS microstrip antenna using multilayer LTCC substrate," *IEEE Antennas Wireless Propag. Lett.*, vol. 9, pp. 421–423, 2010.
[21] T. S. Ooi, S. K. A. Rahim, A. Y. Abdulrahman, B. P. Koh, and S. K. Lee, "Compact dual-band circularly polarized patch antenna with bandwidth enhancement," *J. Optoelectron. Adv. Mater.*, vol. 13, no. 10, pp. 1279–1284, Oct. 2011.
[22] N. Zakaria, S. K. A. Rahim, T. S. Ooi, K. G. Tan, A. W. Reza, and M. S. A. Rani, "Design of stacked microstrip dual-band circular polarized antenna," *Radioengineering*, vol. 21, no. 3, pp. 875–880, Sep. 2012.
[23] C. Deng, Y. Li, Z. Zhang, G. Pan, and Z. Feng, "Dual-band circularly polarized rotated patch antenna with a parasitic circular patch loading," *IEEE Antennas Wireless Propag. Lett.*, vol. 12, pp. 492–495, 2013.
[24] K. Chen, J. Yuan, and X. Luo, "Compact dual-band dual circularly polarised annular-ring patch antenna for BeiDou navigation satellite system application," *IET Microw., Antennas Propag.*, vol. 11, no. 8, pp. 1079–1085, Jun. 2017.
[25] Z. Wang, R. She, J. Han, S. Fang, and Y. Liu, "Dual-band dual-sense circularly polarized stacked patch antenna with a small frequency ratio for UHF RFID reader applications," *IEEE Access*, vol. 5, pp. 15260–15270, 2017.
[26] Y.-K. Jung and B. Lee, "Dual-band circularly polarized microstrip RFID reader antenna using metamaterial branch-line coupler," *IEEE Trans. Antennas Propag.*, vol. 60, no. 2, pp. 786–791, Feb. 2012.
[27] C. G. M. Ryan and G. V. Eleftheriades, "Single- and dual-band transparent circularly polarized patch antennas with metamaterial loading," *IEEE Antennas Wireless Propag. Lett.*, vol. 14, pp. 470–473, 2015.
[28] R. Khajeh Mohammad Lou, M. Naser-Moghadasi, and R. A. Sadeghzadeh, "Compact multi-band circularly polarized CPW fed antenna based on metamaterial resonator," *Wireless Pers. Commun.*, vol. 94, no. 4, pp. 2853–2863, Jun. 2017.

MOHAMMED A. AL-MIHRAB was born in Telafer, Nineveh, Iraq, in 1988. He received the B.Sc. degree in electrical engineering from the University of Mustansiriya, Baghdad, Iraq, in 2011, and the M.Sc. degree in electronics and communication engineering from Cankaya University, Ankara, Turkey, in 2014, where he is currently pursuing the Ph.D. degree in electronic and communication engineering. His research interests include microwave circuits, circular polarization antennas, and power electronic devices.

ALI J. SALIM was born in Baghdad, Iraq, in 1975. He received the B.Sc. degree in electrical engineering and the M.Sc. degree in communication engineering from the University of Baghdad, Iraq, in 1999 and 2002, respectively, and the Ph.D. degree in communication engineering from the University of Technology, Iraq, in 2011. He has three patents. He has published more than 45 papers in international and local conferences and journals in the field of design and miniaturization of microstrip and printed antennas, wearable textile antenna design, compact BPF microwave filter design, substrate integrated waveguide (SIW) technology for microwave antennas and filters design, and antennas diversity for MIMO wireless applications.

JAWAD K. ALI (Senior Member, IEEE) was born in Baghdad, Iraq, in November 1956. He received the B.Sc. and M.Sc. degrees from the Al-Rasheed College for Science and Technology, Iraq, in 1979 and 1986, respectively, and the Ph.D. degree in communication and electronics engineering, in 2018. From 1989 to 1991, he joined a Ph.D. Study Program with the AZMA Academy, Brno, Czechoslovakia. Since 2010, he has been a Professor of microwave engineering with the University of Technology, Iraq, where he is currently the Founder and the Head of the Microwave Research Group. He has served as the Vice President of the University of Technology for Scientific Affairs and Postgraduate Studies, till December 2019. He is also the Dean of the Communication Engineering Faculty, University of Technology, Iraq. He has more than 100 published papers in local and international conferences and peer-reviewed journals. His research interests include microwave antenna miniaturization and design, passive microwave circuits design, and FPGA-based system design. He is a member of IET and IEICE. He is also the Editor-in-Chief and a member of the editorial boards of many national and international journals.